# Axial band scaling for bidisperse mixtures in granular tumblers

G. Juarez,[1] J. M. Ottino,[2,3,4] and R. M. Lueptow[4,*]

[1]*Department of Physics and Astronomy, Northwestern University, Evanston, Illinois 60208, USA*
[2]*Department of Chemical and Biological Engineering, Northwestern University, Evanston, Illinois 60208, USA*
[3]*The Northwestern Institute on Complex Systems (NICO), Northwestern University, Evanston, Illinois 60208, USA*
[4]*Department of Mechanical Engineering, Northwestern University, Evanston, Illinois 60208, USA*

Axial banding in rotating tumblers has been experimentally observed, but the dependence of band formation on the relative concentration of the bidisperse particles has not been thoroughly examined. We consider axial band formation and coarsening for dry and liquid granular systems of bidisperse mixtures of glass beads where the small particle volume fraction ranges from 10% to 90% in half-filled tumblers for several rotation rates. Single bands form for small particle volume fractions as low as 10% and as high as 90%, usually near the end walls. Band formation along the entire length of the tumbler is less likely at very low or very high volume fractions. After many rotations the segregation pattern coarsens, and for small particle volume fractions of 50% and greater, the coarsening is logarithmic. For very low or very high small particle volume fractions, the rate of coarsening is either not logarithmic or coarsening does not occur within the duration of the experiment (600 rotations). When bands form, the width of the band for either the small or large particles scales with the tumbler diameter.

PACS number(s): 45.70.−n, 47.57.Gc

## I. INTRODUCTION

It is well known that a bidisperse mixture of granular particles will segregate when external forcing is applied. A partially filled rotating tumbler is often used as a canonical system for the study of granular segregation, and the external energy is applied in the form of angular rotation. For an initially well-mixed system of particles in a long tumbler rotating about its axis, the smaller particles percolate to lower levels in the flowing layer as they flow through it. After a few rotations, radial segregation reaches steady state, with small or dense particles at the center of the bed surrounded by large or less dense particles [1–10]. Particles then segregate axially to form bands of alternating particle types along the entire length of the tumbler [11–19].

Axial band formation is a robust characteristic of a size varying bidisperse mixture, and it depends on several parameters. The geometry of the tumbler [20–23], particle size ratio [20,24,25], interstitial fluid [22,26–28], rotation rate [20,22,24–26,28–31], particle elasticity [24,31], and fill level [24,29,31] can all affect band formation to some extent. Yet, it is unclear how the relative concentration of small and large particles impacts band formation. Nearly all experiments presented to date have been performed with relative particle volume fractions of either 1:1 or 1:2, since these are favorable conditions for observing axial segregation.

A few aspects are well established. For bidisperse particles in a long tumbler, the first axial bands appear between $O(10)$ to $O(100)$ rotations after radial segregation occurs, usually near the end walls. The time at which these bands first appear depends on the parameters listed above. The connection between radial and axial segregation is unclear, but it appears that radial segregation is a necessary precondition

for axial segregation to ensue. Axial segregation is believed to occur as a result of the difference in the dynamic angle of repose of the two different particle types [6,15,19,30,32], where the angle of repose is related to the size, density, and coefficient of friction of the particles. Initially, bands can split, merge, or remain stable. If the tumbler rotates for a long time the bands typically merge, so that the pattern coarsens. Dry and liquid granular systems (DGS, LGS) have several similarities and yet some subtle differences. Liquid systems usually form bands more quickly than dry systems [26]. Traveling waves appear when air is the interstitial fluid, but not when the interstitial fluid is a liquid [22,33]. However, bands in dry and liquid granular systems both coarsen at a logarithmic rate [22,27,34], and simulations using a continuum description also show a logarithmic coarsening rate for axial segregation patterns in long rotating tumblers [35,36].

The objective of this study is to explore the parameter space for band formation in terms of the relative concentration of small and large particles as well as the rotational speed and interstitial fluid. Our goal is to determine the range of conditions for which bands form and the nature of the bands and their dynamics once they form. We consider how the number of bands, the surface area of the bands, and the coarsening rate depends on the relative fractions of small and large particles. Furthermore, by varying the relative fractions of the two particle types, we can also consider the fundamental scaling for the bandwidth and wavelength, properties that have not been previously examined in detail.

## II. EXPERIMENTAL METHODS

A horizontal acrylic tube of length 75 cm and inner diameter $D=6.35$ cm was partially filled with a bidisperse mixture of glass beads and rotated about its axis by a dc stepper motor with a planetary gear drive controlled by a computer.

*r-lueptow@northwestern.edu

Dry experiments, with air as the interstitial fluid, were performed using a bidisperse mixture of $d_S$=0.6 mm (0.57±0.08 mm) silver Ceroglass® beads and $d_L$=2 mm (2.0±0.06 mm) black basalt beads ($d_L/d_S$=3.33). Liquid granular experiments used tap water as the interstitial fluid with a few drops of detergent to reduce the surface tension so that the smaller beads would not become trapped in air bubbles in the tube. These experiments used the same 0.6 mm silver Ceroglass® beads with 2 mm black basalt beads and another mixture of 1 mm (0.99±0.11 mm) clear glass beads with 2 mm (2.0±0.06 mm) black basalt beads ($d_L/d_S$=2).

The fill level of the tube was approximately 50%, based on the fraction of the tube volume that was filled with particles when the tube was in a vertical position. The percentage of small particles varied as 10%, 20%, 25%, 30%, 34%, 50%, 66%, 70%, 75%, 80%, and 90%. Filling the tube with the proper volume of each particle type required special care. A graduated cylinder was used to measure the volume of each particle type so that when added together the total volume of the two types of beads would be one-half the volume of the tumbler. Since a bidisperse mixture packs more efficiently than monodisperse beads, the final fill level of the bidisperse mixture was slightly less than one-half of the tumbler volume, typically 47% to 49% full. Pouring the particles into the tumbler can cause them to segregate, therefore the tumbler was shaken horizontally to ensure a homogeneous mixture throughout the tube before beginning each experiment.

The angular rotation speeds, $\omega$, were chosen so that the flowing layer remained in the continuous cascading flow regime with a nearly flat free surface [37–40]. For the LGS, the angular speeds were 5, 10, 15, and 20 RPM, corresponding to Froude numbers, $Fr=\omega^2 R/g$, of $8.81\times10^{-4}\leq Fr \leq 1.41\times10^{-2}$, where $R$ is the radius of the tube, and $g$ is the acceleration of gravity. For the DGS, the angular speeds were 10, 15, 20, 25, 30, 35, and 40 RPM, corresponding to $3.52\times10^{-3}\leq Fr \leq5.63\times10^{-2}$.

A digital camera was synchronized with the stepper motor that drives the tumbler to acquire images of the fixed bed of particles as viewed from the side of the tumbler at the same angular position with each revolution of the tumbler. The camera was positioned perpendicular to the axis of the tumbler, approximately 4 m from the experimental setup, so that the image included the entire length of the side of the tumbler. A fluorescent light was aligned parallel to the tumbler to illuminate the fixed bed.

Space-time plots were generated to track the evolution of band formation within the tumbler. Images of the side of the tumbler were cropped so that only the bottom of the tumbler to the top edge of the fixed bed remained in the image. The image intensity was averaged in the vertical direction (parallel to bands) to provide the average intensity as a function of the position along the length of the tumbler, with high intensity corresponding to small clear or silver beads and low intensity corresponding to large black beads. Space-time plots were created for a total of 600 tumbler rotations by stacking single pixel thick lines of the average intensity with time progressing from top to bottom. A thresholding algorithm was used to process the space-time plot converting

from gray scale to black and white in order to enhance clarity while keeping the enhanced space-time plot as close to the original as possible. The goal was to avoid confusion as to whether the brightness of the band was due to a more densely packed band of smaller particles or the color of the particles. In all cases, the lighter colored particles in the space-time plots are the smaller of the two particles in the mixture.

## III. RESULTS

### A. Space-time plots

Over 160 space-time plots are presented in matrix form as a function of the small particle volume fraction and the angular velocity of the tumbler. The matrix of space-time plots for the liquid granular mixture of 0.6 and 2 mm glass beads is shown in Fig. 1(a). Bands do not form for low small particle volume fractions, and this result is enhanced at low angular speeds. Similarly, bands do not form at very high small particle volume fractions, especially at the highest angular speed. In the upper half of the matrix, for a particular small particle volume fraction, the number of axial bands increases with increasing RPM. In the lower half of the matrix, for higher small particle fractions, the initial number of bands is approximately the same for each run. Bands of large particles are thinner as the angular velocity increases. These large particle bands merge for small particle volume fractions of 50% to 80%. The extent of merging is somewhat dependent on the angular velocity with generally fewer merges at higher angular velocities.

The matrix of space-time plots for the liquid granular mixture of 1 and 2 mm glass beads is shown in Fig. 1(b). Axial segregation is evident within the duration of the run for all volume fractions and angular velocities except for one case (10% small particles, 5 RPM). Bands form more slowly at low small particle volume fractions than at other volume fractions. Below 50% small particle fraction, band merging is rare, while it is quite common above 50%. Finally, a unique characteristic of this mixture is that for the angular velocity of 5 RPM, at volume fractions of 34% to 90%, there are instabilities, or oscillations, of particle bands that occur before stable bands form, consistent with previous results for 0.55 and 1.5 mm ($d_L/d_S$=2.72) beads at a 50% small particle fraction [34]. As the small particle fraction increases, the oscillations and instabilities tend to last longer, delaying stable band formation.

Space-time plots for the dry mixture of 0.6 and 2 mm glass beads, shown in Fig. 2, indicate significant band formation for a much smaller range of small particle volume fractions: From 34% to 70%. At low small particle volume fractions, bands form more readily for higher angular velocities, whereas at high volume fractions, band formation occurs more readily at lower angular velocities. Merging of bands occurs for small particle volume fractions of 50% to 70% where band formation is prominent. An interesting characteristic of this system is the appearance of traveling waves. For low angular velocities and small particle volume fractions of 66% to 75%, traveling waves similar to those found previously [22,33] are observed.
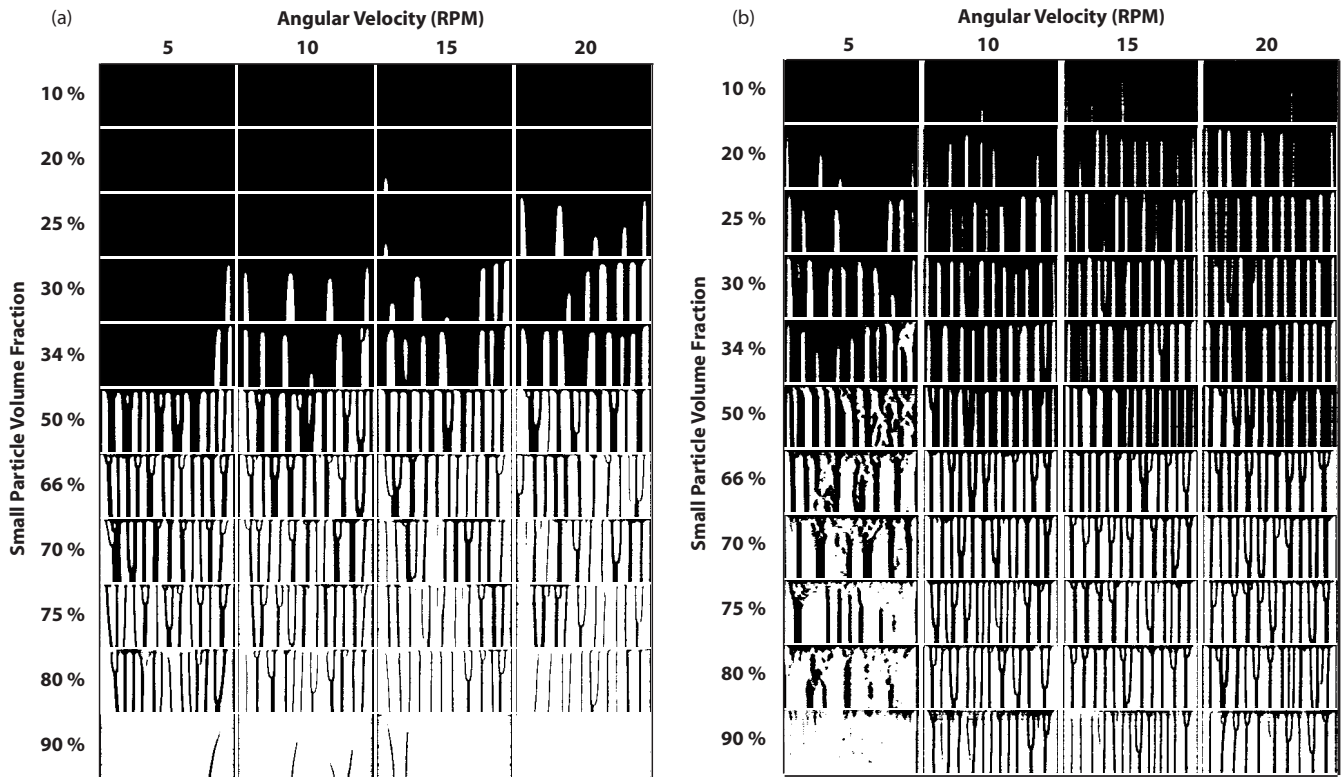
FIG. 1. The matrix of space-time portraits for both of the liquid granular systems (LGS) show band formation as a function of the fraction of small particle volume and angular velocity for 600 tumbler rotations. In each cell, time progresses from top to bottom. (a) Mixture is 0.6 mm (light) and 2.0 mm (dark) glass beads ($d_L/d_S$=3.33). (b) Mixture is 1.0 mm (light) and 2.0 mm (dark) glass beads ($d_L/d_S$=2).

Although dry mixtures of 1 and 2 mm beads were tested, band formation was not observed for any small particle fraction. This may be related to the ratio of the tumbler diameter to average particle diameter. Previous experimental results for dry systems with a small particle fraction of 50% indicate that segregation always occurs for ratios above 55, never occurs for ratios below 40, and depend on angular velocity for ratios in between [20]. For the 0.6 and 2 mm mixture the ratio is 49, while for the 1 and 2 mm mixture the ratio is 42. Of course, it is likely that the interstitial fluid and small particle fraction also play roles in the ratio at which segregation occurs.

Clearly, axial band formation is dependent on the small particle fraction. Band formation is also easily affected by the particle size ratio and the interstitial fluid. Merging of bands occurs for both dry and liquid granular systems, although for the liquid system only large particle (dark) bands merge. In the dry system, both small (light) and large (dark) particle bands merge. There also appears to be a minimum width for a band to be stable, as discussed in a later section.

### B. Band evolution

Band formation and evolution can also be evaluated by considering the fraction of the small particle surface area visible in the image of the fixed bed and the number of small particle bands as a function of time or rotations. The fraction of small particles visible in the fixed bed and the number of small particle bands are calculated using an algorithm similar to that used to create the space-time plots. For each revolution, the fraction of the vertically averaged intensity along the length of the tumbler for small particles, which represents the fraction of area occupied by small particles, is obtained. This fraction is plotted as a function of tumbler rotations, as shown in Figs. 3(a) and 3(c). For the 0.6 and 2 mm liquid granular mixture, Fig. 3(a), the surface area reaches a constant value within about $O(50)$ rotations for small particle volume fractions of 50% and greater. For fractions less than 50%, the appearance of bands is delayed. When the bands appear, the surface area increases at a slower rate than for higher fractions up to about $O(200)$ rotations, and then increases at an even slower rate. As expected, the fraction of surface area increases as the small particle volume fraction increases. Also, for a given particle fraction, the surface area fraction increases as the angular velocity increases (not shown). Band formation and coarsening follow two different trends depending on the small particle volume fraction, as shown in Fig. 3(b). At high volume fractions, 50%–80%, bands form quickly and later show logarithmic coarsening, similar to the results of Fiedor and Ottino [22]. The coarsening is of the form, $-k \ln(n)$, where $n$ is the number of rotations with $k$=2.1. For lower volume fractions of 30% and 34% as well as for 90%, segregation patterns do not coarsen. As the angular velocity increases, the behavior of both groups remains nearly the same (not shown).

Results are similar for the 1 and 2 mm liquid granular mixture, as shown in Figs. 3(c) and 3(d) except that the 50% mixture falls into the same category as the lower volume
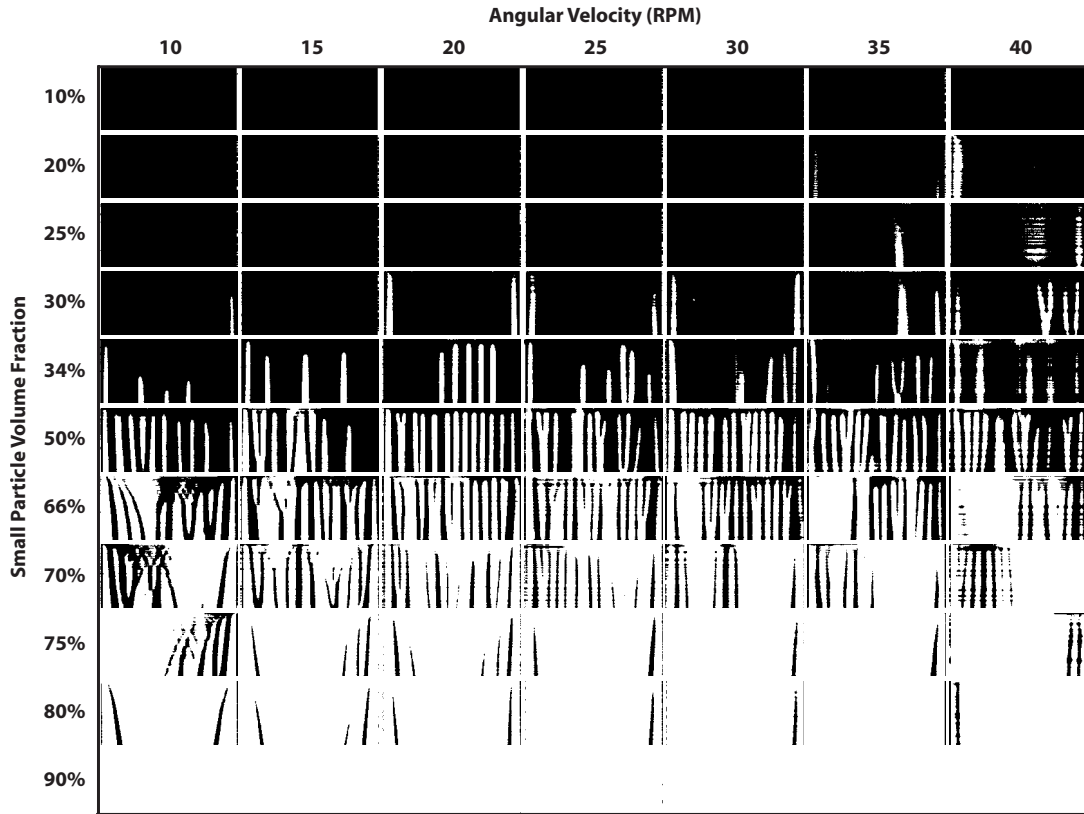
FIG. 2. The matrix of space-time portraits for the dry granular system (DGS) shows band formation as a function of the fraction of small particle volume and angular velocity for 600 tumbler rotations. Mixture is 0.6 mm (light) and 2.0 mm (dark) glass beads ($d_L/d_S$=3.33).

fraction mixtures. The initial transient for the fraction of surface area to reach a nearly constant value for volume fractions of 66% and greater is from $O(50)$ to $O(100)$ rotations. For volume fractions of 50% or less, the transient is much longer, around $O(150)$ to $O(400)$ rotations. For a given angular velocity, the percent surface area increases as the small particle fraction increases, as it did for the 0.6 and 2 mm liquid mixture, although for a given volume fraction, the surface area fraction does not increase as angular velocity increases (not shown). Again the band formation and coarsening character can be categorized into two groups: Relatively fast band formation followed by logarithmic coarsening at high small particle volume fractions; and slow band formation with no coarsening at low volume fractions. For volume fractions of 66% to 90%, segregation patterns coarsen at a logarithmic rate with $k=3.1$. As the angular velocity increases, the behavior remains the same (not shown).

Finally for the 0.6 and 2 mm dry mixture, the initial transient for the fraction of surface area of small particles is faster for volume fractions of 50% and greater (not shown). Constant surface area is reached at $O(50)$ to $O(100)$ rotations. For volume fractions of 34% or less, the transient lasts from $O(150)$ to $O(250)$ rotations. Again the fraction of surface area increases as small particle volume fraction increases, but the surface area fraction does not change with the angular velocity. The number of bands is again split into two groups, a group for which bands form quickly and a group that does not (not shown). The first group includes
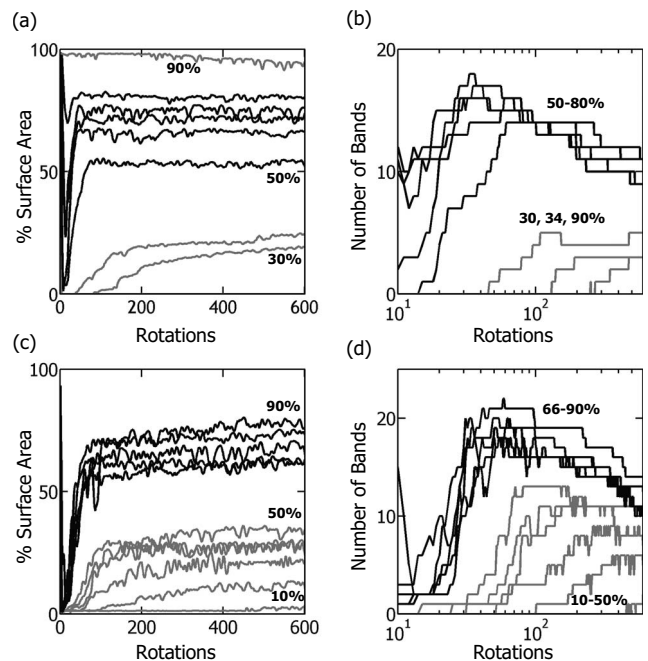


FIG. 3. Evolution of the bands in terms of (a) the fraction of surface area of small particles and (b) the total number of bands for the LGS mixture of 0.6 and 2 mm at 10 RPM. (c) Fraction of surface area of small particles and (d) total number of bands for the LGS mixture of 1 and 2 mm at 10 RPM. Dark curves are for small particle fractions that undergo logarithmic coarsening. Volume fractions are indicated on the plots.
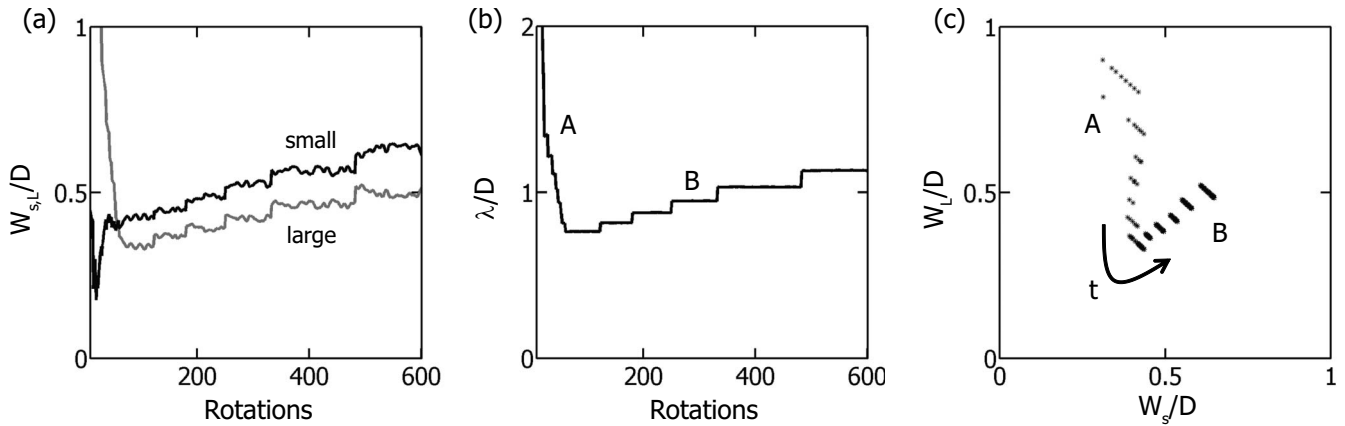
FIG. 4. Evolution of the bandwidth and average wavelength for a LGS of 0.6 and 2.0 mm particles at a 50% small particle volume fraction is shown for 10 RPM. (a) After an initial transient, the average small and large bandwidths increase with time. (b) The average wavelength increases as a function of time after the initial transient. (c) A scatter plot of the large and small average bandwidths shows that the bandwidths are of the order of the tumbler diameter. All values are normalized by the tumbler diameter.

concentrations of 50%, 66%, and 70%. The experiments may not have been long enough to observe coarsening, but coarsening would not be expected below $O(600)$ rotations [22]. Only a small number of bands form at other concentrations, and they do so slowly.

### C. Wavelength and bandwidth

The upper half of the space-time matrix plots in Figs. 1 and 2 show that the widths of the small particle bands are nearly identical regardless of the angular velocity or particle volume fraction. Similarly, on the lower half of the matrix, the widths of large particle bands are nearly the same, but are thinner than the widths of the small particle bands. To examine this, we define the average bandwidths of small, $W_S$, and large, $W_L$, particles. Knowing the individual bandwidths, it is then easy to calculate the wavelength for the system. For example, these values can be calculated for the 0.6 and 2 mm liquid system, 50% small particle volume fraction at 10 RPM, as shown in Fig. 4.

The ratio of the average bandwidth of small and large particles to the tumbler diameter is plotted as a function of tumbler rotations in Fig. 4(a). The average widths of small and large particle bands are less than one tumbler diameter. Furthermore, both display a steplike change in time, corresponding to band merging. As coarsening takes place, the number of bands decreases, so the average bandwidth for both small and large particles increases with time. The ratio of the average wavelength, $\lambda = W_L + W_S$, to the tumbler diameter is shown in Fig. 4(b). The average wavelength is initially quite large, but drops quickly to a wavelength that is slightly less than the tumbler diameter as the individual bands of small particles form [A in Fig. 4(b)]. Gradually, the wavelength increases as the segregation pattern coarsens [B in Fig. 4(b)], but the wavelength remains the same order of magnitude as the tumbler diameter, consistent with previous results [21].

The dimensionless average bandwidth of large particles is plotted against the dimensionless average bandwidth of small particles in Fig. 4(c) to show the evolution of the segregation pattern. In the figure, time progresses from top left to bottom right, indicating that the system is initially dominated by wide bands of large particles. This is consistent with the first stage being radial segregation with most small particles located in the core. As time progresses, bands of small particles form [A in Fig. 4(b)]. These new bands have about the same width, $W_S/D \approx 0.45$, but their appearance forces the bands of large particles to narrow, corresponding to A in Fig. 4(c). After about 50 rotations, no more small particle bands form, but the segregation pattern coarsens [B in Fig. 4(b)]. During the coarsening, the bandwidths of both small and large particles increase, as shown in Fig. 4(a), resulting in region B in Fig. 4(c). Each series of data points along a line in Fig. 4(c) corresponds to changing bandwidths, and the jumps between individual lines of data points correspond to the formation of a new band or to a merging of bands. There are six jumps between lines [A in Fig. 4(c)] corresponding to six step changes in wavelength [A in Fig. 4(b)], each related to the appearance of a new band of small particles. There are five jumps between bands [B in Fig. 4(c)] corresponding to five merges [B in Fig. 4(b)]. The lines are sloped because the small particle bands widen as the large particle bands narrow in between events of bands appearing or merging. This effect is quite apparent in the bandwidths shown in Fig. 4(a) for merge events appearing at more than 100 rotations.

Similar results occur for conditions presented in Figs. 1 and 2 where bands form and coarsen. For example, when the small particle volume fraction is high, as shown in Fig. 5(a) corresponding to 90% small particle fraction for the $d_L/d_S = 2$ mixture at 10 RPM, the large particle bands start quite wide, but decrease in width as small particle bands form [A in Fig. 5(a)]. Once the bands have formed, the bands of large particles merge but do not increase in width. On the other hand, bands of small particles get wider [B in Fig. 5(a)] as coarsening progresses. Thus, in the scatter plot of $W_S$ and $W_L$ time progresses very rapidly from top left to bottom left, and then moves slowly from bottom left to bottom right.

Other scenarios take place when coarsening does not occur. When the small particle volume fraction is low, as
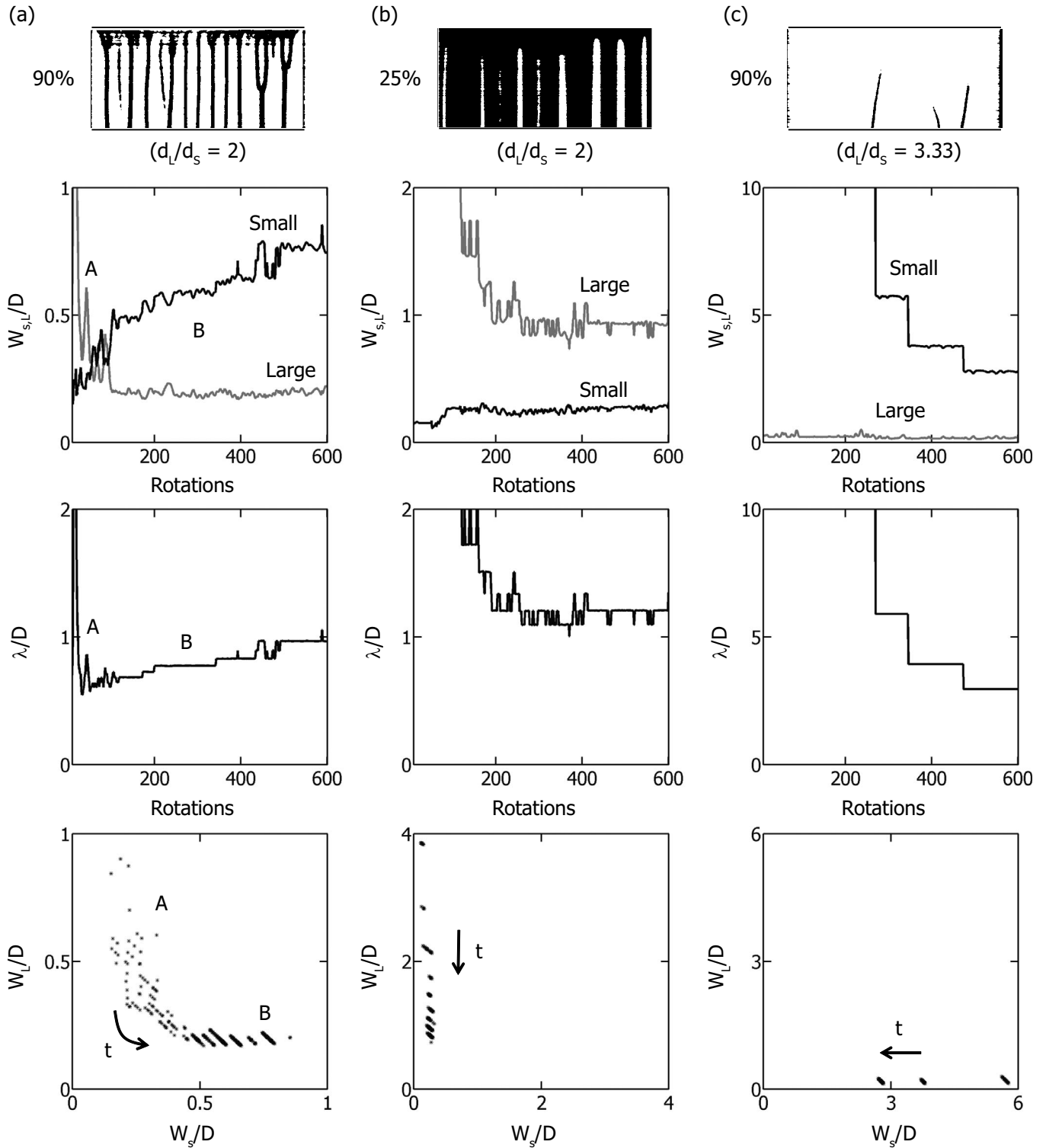
FIG. 5. Space-time plots, the average bandwidth of small and large particles, and the wavelength depend on the relative volume fractions of small and large particles. The average small and large bandwidth are plotted against one another in the lowest row. All cases are LGS.

shown in Fig. 5(b), corresponding to 25% small particle fraction for the $d_L/d_S=2$ mixture at 10 RPM, the average width of small particle bands remains nearly constant in time after the bands have formed. The width of large particle bands decreases as new bands of small particles appear. However, the bandwidth of the small particle bands is constant. As a result, when the average bandwidth of small and large par-

ticles are plotted against one another, the width of small particle bands does not change as time progresses.

The opposite situation occurs when the small particle fraction is high and small particles initially saturate the surface, as shown in Fig. 5(c), corresponding to 90% small particle fraction for the $d_L/d_S=3.33$ mixture at 10 RPM. Bands form only after many rotations and once large particle bands
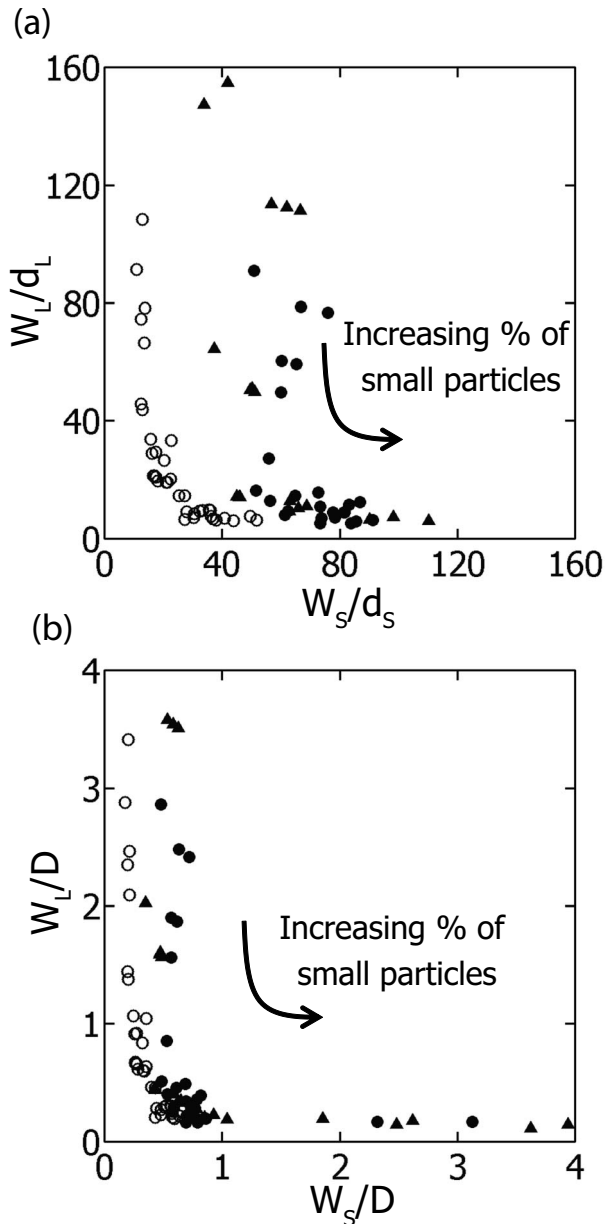
FIG. 6. (a) Scatter plot of the average band width of small and large particles $W_{S,L}$ divided by the particle diameters, $d_S, d_L$ for all systems studied does not collapse the data. (b) The average band widths of small and large particles $W_{S,L}$ divided by the tumbler diameter, $D$, are quite similar suggesting that band widths scale with the tumbler diameter. Symbols: $d_L/d_s=3.33$, ● LGS, ▲ DGS; $d_L/d_s=2$: ○ LGS.

form, their bandwidth remains constant in time. In the scatter plot, time progresses from right to left as bands of large particles of constant width form due to the appearance of very narrow bands of small particles.

An alternative to considering how the bandwidth for a specific small particle volume fraction evolves in time is to plot the bandwidth for all particle fractions at a particular point in time. The bandwidth at 600 rotations for all of the dry and liquid experiments is shown in Fig. 6(a). In this case the dimensionless bandwidth, $W_{S,L}/d_{S,L}$, is defined as the ratio of the average bandwidth of small (large) particles to the

diameter of the small (large) particles, similar to Kuo *et al.* [24,31]. As the small particle volume fraction increases (moving from the top left-hand corner to the bottom right-hand corner of the graph) the small particle (light) bands increase in width, while the large particle (dark) bands approach a constant value. The bandwidth can vary substantially when measured in terms of particle diameters ranging from about five particle diameters to nearly 160 particle diameters. Clearly, the data do not collapse, but the data points for the 0.6 and 2 mm dry and liquid granular mixtures lie almost on top of each other. Using an alternative dimensionless bandwidth, $W_{S,L}/D$, the ratio of the average bandwidth of small (large) particles to the tumbler diameter, results in better collapse of the data, as shown in Fig. 6(b). This suggests that the tumbler diameter is the proper scale for the average width of the bands. Although it is difficult to extract numerical data from previous studies at conditions comparable to the ones used here, a qualitative examination of space-time plots confirms this scaling [22,24,29,31].

From Fig 6(b), it appears that after some time at least one of the bandwidths approaches $0.2D$ to $0.7D$, regardless of the size of the other band. That is, in the upper portion of Fig. 6(b), which corresponds to low small particle concentrations, the few small particle bands that form have a width of $0.2D$ to $0.7D$, while the large particles, which are much more plentiful, form very wide bands to fill in between the small particle bands. Likewise, in the lower right-hand corner for high small particle volume fractions, the few large particle bands that form have a width of about $0.2D$, while the small particle bands are quite wide to fill in the space in between. In both of these cases there is very little coarsening, probably because the bands of the less prevalent particle size are so far apart. However, for the cases where neither particle size dominates, which appear in the lower left-hand corner for $W_L/D < 1$ and $W_S/D < 1$, coarsening is typically observed.

## IV. CONCLUSIONS

Axial band formation and evolution is strongly affected by the relative volume fraction of small and large particles. Several conclusions can be drawn. The relative volume fraction of particles determines the rate at which bands form, the number of bands that form, and whether or not merging of bands occurs. Axial bands form well outside the range of small particle fractions of 50%-66% typically used in experiments. The particle size ratio and the interstitial fluid significantly alter the range in which axial segregation occurs. Band formation and evolution can be grouped into two categories: The well-known band formation along the entire length of the tumbler followed by logarithmic coarsening; and a situation that occurs for low or high small particle fractions where relatively few bands form slowly and coarsening does not occur. There is a minimum critical bandwidth that occurs when bands persist in the system. The critical bandwidth scales with the tumbler diameter and is similar for all granular systems at $0.2D$ to $0.7D$.

While this paper clarifies some aspects of the dependence of granular band formation, width, and coarsening on the relative volume fraction of the two particles and other studies

have determined the effect of other parameters on band formation, questions remain. Foremost is how bands are initiated. Heuristic explanations of axial particle segregation and the related band formation depend on differences in the angle of repose for the two particle species. But it is not clear how these different angles of repose initially appear. Likewise the impact of the endwalls on band formation is unclear, though results for low and high small particle fractions show that when just few bands form, they always form near the ends of the tumbler, suggesting that the endwalls play a significant role. It appears that bidisperse granular mixtures exhibit different types of phase separations analogous to nucleation for extreme values of small particle fraction and spinodal decomposition for moderate small particle fractions. A possible approach to better understand this may be to use particle dynamics simulations in which the motion of each type of particle can be followed in detail.

[1] J. Duran, *Sands, Powders, and Grains* (Springer, New York, 2000).
[2] C. M. Dury and G. H. Ristow, J. Phys. I (France) **7**, 737 (1997).
[3] D. V. Khakhar, J. J. McCarthy, T. Shinbrot, and J. M. Ottino, Phys. Fluids **9**, 31 (1997).
[4] D. V. Khakhar, J. J. McCarthy, and J. M. Ottino, Phys. Fluids **9**, 3600 (1997).
[5] K. M. Hill, D. V. Khakhar, J. F. Gilchrist, J. J. McCarthy, and J. M. Ottino, Proc. Natl. Acad. Sci. U.S.A. **96**, 11701 (1999).
[6] K. M. Hill, A. Caprihan, and J. Kakalios, Phys. Rev. Lett. **78**, 50 (1997).
[7] F. Cantelaube and D. Bideau, Europhys. Lett. **30**, 133 (1995).
[8] E. Clement, J. Rajchenbach, and J. Duran, Europhys. Lett. **30**, 7 (1995).
[9] I. S. Aranson and L. S. Tsimring, Rev. Mod. Phys. **78**, 641 (2006).
[10] N. Thomas, Phys. Rev. E **62**, 961 (2000).
[11] M. B. Donald and B. Roseman, Br. Chem. Eng. **7**, 749 (1962).
[12] Y. Oyama, Sci. Pap. Inst. Phys. Chem. Res. **37**, 17 (1940).
[13] M. Nakagawa, Chem. Eng. Sci. **49**, 2540 (1994).
[14] O. Zik, D. Levine, S. G. Lipson, S. Shtrikman, and J. Stavans, Phys. Rev. Lett. **73**, 644 (1994).
[15] S. D. Gupta, D. V. Khakhar, and S. K. Bhatia, Chem. Eng. Sci. **46**, 1513 (1991).
[16] D. Levine, Chaos **9**, 573 (1999).
[17] J. Stavans, J. Stat. Phys. **93**, 467 (1998).
[18] N. Taberlet, M. Newey, P. Richard, and W. Losert, J. Stat. Mech.: Theory Exp. (2006) P07013.
[19] T. Elperin and A. Vikhansky, Phys. Rev. E **60**, 1946 (1999).
[20] A. Alexander, F. J. Muzzio, and T. Shinbrot, Granular Matter **5**, 171 (2004).
[21] C. R. J. Charles, Z. S. Khan, and S. W. Morris, Granular Matter **8**, 1 (2006).

[22] S. J. Fiedor and J. M. Ottino, Phys. Rev. Lett. **91**, 244301 (2003).
[23] S. J. Fiedor, P. Umbanhowar, and J. M. Ottino, Phys. Rev. E **73**, 041303 (2006).
[24] H. P. Kuo, R. C. Hsu, and Y. C. Hsiao, Powder Technol. **153**, 196 (2005).
[25] K. M. Hill and J. Kakalios, Phys. Rev. E **52**, 4393 (1995).
[26] N. Jain, D. V. Khakhar, R. M. Lueptow, and J. M. Ottino, Phys. Rev. Lett. **86**, 3771 (2001).
[27] S. J. Fiedor, P. Umbanhowar, and J. M. Ottino, Phys. Rev. E **76**, 041303 (2007).
[28] T. Finger and R. Stannarius, Phys. Rev. E **75**, 031308 (2007).
[29] T. Arndt, T. Siegmann-Hegerfeld, S. J. Fiedor, J. M. Ottino, and R. M. Lueptow, Phys. Rev. E **71**, 011306 (2005).
[30] K. M. Hill and J. Kakalios, Phys. Rev. E **49**, R3610 (1994).
[31] H. P. Kuo, Y. C. Hsiao, and P. Y. Shih, Powder Technol. **166**, 161 (2006).
[32] J. Bridgwater, N. W. Sharpe, and D. C. Stocker, Trans. Inst. Chem. Eng. **47**, T114 (1969).
[33] K. Choo, T. C. A. Molteno, and S. W. Morris, Phys. Rev. Lett. **79**, 2975 (1997).
[34] T. Finger, A. Voigt, J. Stadler, H. G. Niessen, L. Naji, and R. Stannarius, Phys. Rev. E **74**, 031312 (2006).
[35] I. S. Aranson and L. S. Tsimring, Phys. Rev. Lett. **82**, 4643 (1999).
[36] I. S. Aranson, L. S. Tsimring, and V. M. Vinokur, Phys. Rev. E **60**, 1975 (1999).
[37] J. M. Ottino and D. V. Khakhar, Annu. Rev. Fluid Mech. **32**, 55 (2000).
[38] J. Rajchenbach, Phys. Rev. Lett. **65**, 2221 (1990).
[39] H. Henein, J. K. Brimacombe, and A. P. Watkinson, Metall. Trans. B **14B**, 191 (1983).
[40] J. Mellmann, Powder Technol. **118**, 251 (2001).